



## Modeling, Control and Simulation of Cascade Control Servo System for One Axis Gimbal Mechanism

M. Abdo<sup>a\*</sup>, A. R. Toloei<sup>b</sup>, A. R. Vali<sup>b</sup>, M. R. Arvan<sup>b</sup>

<sup>a</sup> Department of Electrical Engineering, Malek-Ashtar University of Technology, Tehran, Iran

<sup>b</sup> Department of Aerospace, Shahid Beheshti University, Tehran, Iran

### PAPER INFO

#### Paper history:

Received 27 March 2013

Received in revised form 27 April 2013

Accepted 20 June 2013

#### Keywords:

Gimbal System  
Rtae Gyro  
Line of Sight  
Stabilization Loop  
Servo System  
DC Motor

### A B S T R A C T

The gimbal stabilization mechanism is used to provide the stability to an object mounted on the gimbal by isolating it from the base angular motion and vibration. The purpose of this paper is to present a model of control servo system for one axis gimbal mechanism using a cascade PID controller. The gimbal torque relationships are derived by taking into consideration the base angular motion. The conventional PID controller and three cascade controller structures are investigated. The servo control loop is built and modelled in MATLAB/Simulink using these controllers. The simulation results are compared and the servo system performance is analysed for each controller in terms of performance criteria. The comparison results prove that a further improved system performance is achieved using I-PD controller as compared to the system performance obtained when the other controllers are utilized. The paper's value lies in designing the servo control system using a modified controller composed of two parallel I-PD controllers related with a switch depending on the base angular rate as a threshold. The results show that the modified system satisfies the desired servo system requirements.

doi: 10.5829/idosi.ije.2014.27.01a.18

## 1. INTRODUCTION

The main purpose of the optical sensing equipment, (such as cameras, television, radars, lasers and navigation instruments) is to point the sensor from a dynamical platform to a fixed or moving surface. For achieving accurate pointing, it is necessary to control the sensor's line of sight (LOS). In such an environment where the equipment is typically mounted on a movable platform (such as aircrafts, missiles seekers, and airborne tracking systems), maintaining sensor orientation toward a target is a serious challenge. An Inertial Stabilization Platform (ISP) or gimbal system is an appropriate way that can solve this challenge [1]. This popularity and increased use in a lot of modern industrial applications have induced researchers' interest in studying, analyzing, and developing gimbal systems. ISPs usually consist of an assembly of structure, bearings, and motors called a gimbal to which a gyroscope, or a set of gyroscopes, is mounted [2]. It has been shown earlier that the jitter on the LOS can be

reduced by mounting the electro optical EO payload on a set of gimbals. Gimbals are precision electro-mechanical assemblies designed primarily to isolate the optical system from the disturbance induced by the operating environment, such as various disturbance torques and body motions [3]. From the viewpoint of control, such a system is built as a servo motion control system which its essential concepts have not changed significantly in the last 50 years. However, the importance and popularity of servo systems in contrast to open loop systems results in the need to improve transient response times, reduce the steady state errors, and reduce the sensitivity to load parameters. The performance of a system depends heavily on the accuracy of plant modelling. It is therefore necessary to capture all the dynamics of the plant and express the plant in analytical form before the design of gimbal assembly is taken up. Thus, in a typical control loop design cycle of any stabilized gimbal platform assembly, modeling of the plant dynamics is an important milestone [3]. As an example about researches interested in obtaining the mathematical model of gimbal assembly, the following can be mentioned. The kinematic and geometrical coupling

\*Corresponding Author Email: [maherabdo74@yahoo.com](mailto:maherabdo74@yahoo.com) (M. Abdo)

relationships for two degrees of freedom gimbal assembly have been obtained for a simplified case when each gimbal is balanced and the gimbale element bodies are suspended about principal axes [4]. Equations of motion for the two axes yaw-pitch gimbal configuration have been discussed on the assumption that the gimbals are rigid bodies and have no mass unbalance [5]. Otlowski et al. has presented a single degree of freedom (SDOF) gimbal operating in a complex vibration environment [6]. Any servo motion control system should have an actuator module that makes the system to actually perform its function. The most common actuator used to perform this task is the DC servomotor which is regarded as one of the main components of servo system [7, 8]. There are a lot of control methods for the servo motors. Akar and Temiz utilized the PID, fuzzy logic control (FLC) and adaptive neuro-fuzzy inference system (ANFIS) [9]. Rigatos estimated the unknown values of the DC motor using an artificial neural network, and designed a controller based on ANFISn [10]. In another study, Rigatos evaluated the performance of the Kalman filter and the particle filter in reconstructing the state of the DCSM and subsequently in using this state estimation in feedback control [11]. It can be realized that the importance of gimbal systems gave rise to their investigation in a lot of papers as mentioned above in addition to another researches indicated in [12-15]. Without doubt, these researches have contributed to the studying and explaining gimbal systems, but the model of such systems is still difficult and complicated to be understood by engineers because the vast majority of these researches have been interested in the two or multi axes gimbal systems. Also, these systems have been investigated considering the inertia cross coupling between axes. Therefore, this paper presents the model of one axis gimbal system in order to simplify the picture of the gimbal systems and to further investigate the properties of this configuration. In another words, this paper forms a primary theoretical base for designing a multi axes gimbal systems. Concerning the control system, although the researchers tried to utilize and apply many different modern techniques to control servo systems, the conventional PID and its constructors are still the most used approach due to their simple structure, cheap costs, simple design and high performance [16]. In this paper, the cascade PID controller is proposed because of several practical advantages [17]. The well-known PI(D) or more precisely the "Cascade PI(D)" controller is very attractive in terms of simplicity and popularity. Numerical simulations have been performed in order to investigate the performance of the designed servo system and to confirm the improvements obtained from the cascade controller in terms of the performance measures; rise time (tr), settling time (ts), maximum overshoot (Mp), and steady state error (ess). The

remainder of the paper is organized as follows. Second section formulates the problem. The mathematical of gimbal motion is derived in third section. In fourth section, the stabilization loop is constructed by introducing the design of the rate gyro, DC motor, the platform, and the controller. The simulation results are analyzed and a modified controller is designed in fifth section. Finally, the conclusion remarks are highlighted.

## 2. PROBLEM FORMULATION

Newton's first law applied to rotational motion asserts that a body does not accelerate with respect to an inertial frame unless a torque is applied. Furthermore, Newton's second law establishes that if a net torque  $T$  is applied to a homogenous rigid mass having a moment of inertia  $J$ , then the body develops an angular acceleration  $\alpha$  [2] according to:

$$T = J\alpha \quad (1)$$

Therefore, in principle, all that required to prevent an object from rotating with respect to inertial space is to ensure that the applied torque is zero. However, despite careful electromechanical design, numerous sources of torque disturbances can act on a real mechanism causing excessive motion or jitter of (LOS). Also, a means for controlling the object so that it can be rotated in response to command inputs is usually required. Therefore, rate or displacement gyros are typically attached to the object to measure the inertial rotation about the axes that require stabilization and control. The gyro is used in a closed-loop servo system to counteract the disturbances and, at the same time, allow the object to be controlled from external command inputs [2]. The single-axis stabilized gimbal is shown in Figure 1. The purpose of the gimbal is to isolate the stabilized object from base rotation, and allow (LOS) to be pointed. The block diagram in Figure 2 shows the gimbal stabilization system. It is typically configured as a rate servo which attempts to null the difference between the rate command input  $\omega_c$  and the angular rate of the gimbal  $\omega_{Ac}$ . When the rate command input is zero or absent, the system attempts to null the total torque applied to the gimbal, which requires that the stabilization closed-loop generate a control torque at the motor that is equal and opposite to the net disturbance torque. From Figure 2, it can be seen that:

$$\frac{\omega_{Ac}}{T} = \frac{1}{J_s} \Rightarrow T = J\omega_{Ac}s = J\dot{\omega}_{Ac} = J\alpha \quad (2)$$

The control loop introduced works as stabilization system when the rate command input  $\omega_c$  is zero, which means that the control system output  $\omega_{Ac}$  must be zero. While this system tries to track the non zero rate command input.

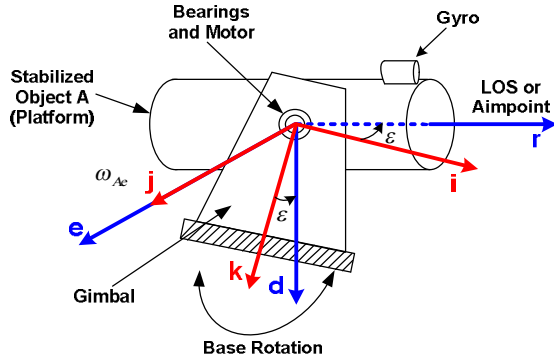


Figure 1. A single-axis gimbal mechanism

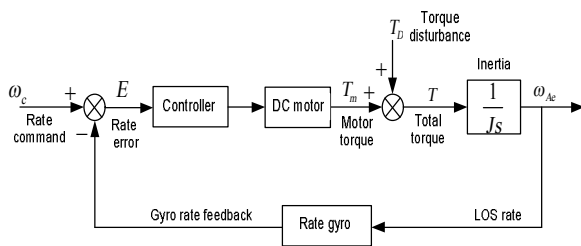


Figure 2. LOS stabilized servo control loop

As a result, the problem can be formulated as follows. The servo control in general can be broken into two fundamental classes. The first class deals with command tracking. It addresses the question that how well does the actual motion follow what is being commanded. The second general class of servo control addresses the disturbance rejection characteristics of the system. Disturbances can be anything from torque disturbances on the motor shaft to incorrect motor parameter estimations used in the feedforward control.

### 3. MATHEMATICAL MODEL OF GIMBAL MOTION

At first, two reference frames are identified ( see Figure 1). Frame  $P$  fixed to the fuselage body (base) with axes  $(i, j, k)$ , and frame  $A$  fixed to the gimbal (stabilized object) with axes  $(r, e, d)$  where  $r$ -axis coincides with the sensor optical axis. The center of rotation is at the origin of the two frames. A transformation between frame  $P$  and  $A$  is made in terms of positive angle  $\epsilon$  (gimbal angle) about the  $e$ -axis:

$${}^A C_P = \begin{bmatrix} \cos \epsilon & 0 & -\sin \epsilon \\ 0 & 1 & 0 \\ \sin \epsilon & 0 & \cos \epsilon \end{bmatrix} \quad (3)$$

The inertial angular velocity vectors of frames  $P$  and  $A$ , respectively are:

$${}^P \bar{\omega}_{P/I} = \begin{bmatrix} \omega_{pi} \\ \omega_{pj} \\ \omega_{pk} \end{bmatrix}, \quad {}^A \bar{\omega}_{A/I} = \begin{bmatrix} \omega_{Ar} \\ \omega_{Ae} \\ \omega_{Ad} \end{bmatrix} \quad (4)$$

where  $\omega_{pi}, \omega_{pj}, \omega_{pk}$  are the base angular velocities of frame  $P$  in relation to inertial space about  $i, j$ , and  $k$  axes respectively, and  $\omega_{Ar}, \omega_{Ae}, \omega_{Ad}$  are the gimbal angular velocities in relation to inertial space about the  $r, e$ , and  $d$  axes, respectively. The inertia matrix of the gimbal is

$${}^A J = \begin{bmatrix} A_r & A_{re} & A_{rd} \\ A_{re} & A_e & A_{de} \\ A_{rd} & A_{de} & A_d \end{bmatrix} \quad (5)$$

where  $A_r, A_e, A_d$  are gimbal moments of inertia about  $r, e$ , and  $d$  axes,  $A_{re}, A_{rd}, A_{de}$  are gimbal moments products of inertia. The angular velocity  $\omega_{Ae}$  is the output of the stabilization loop (servo control system), the purpose of which is to make it possible to keep  $\omega_{Ae} = 0$  despite disturbances, and by that keep the sensor nonrotating in inertial space [5].  $\omega_{Ae}$  can be measured by a rate gyro placed on the gimbal. Utilizing (3), the angular velocities of the stabilized object are:

$$\begin{aligned} \omega_{Ar} &= \omega_{pi} \cos \epsilon - \omega_{pk} \sin \epsilon & (a) \\ \omega_{Ae} &= \omega_{pj} + \dot{\epsilon} & (b) \\ \omega_{Ad} &= \omega_{pi} \sin \epsilon + \omega_{pk} \cos \epsilon & (c) \end{aligned} \quad (6)$$

In [5], by Newton's second law, the external kinematic torques applied to the body  $A$  can be written as follows:

$$\bar{T} = \frac{d}{dt} ({}^A \bar{H}) + {}^A \bar{\omega}_{A/I} \times {}^A \bar{H} \quad (7)$$

where  ${}^A \bar{H}$  is the angular momentum given by:

$${}^A \bar{H} = {}^A J \cdot {}^A \bar{\omega}_{A/I} \quad (8)$$

$${}^A \bar{H} = \begin{bmatrix} A_r \omega_{Ar} + A_{re} \omega_{Ae} + A_{rd} \omega_{Ad} \\ A_e \omega_{Ar} + A_e \omega_{Ae} + A_{de} \omega_{Ad} \\ A_{rd} \omega_{Ar} + A_{de} \omega_{Ae} + A_d \omega_{Ad} \end{bmatrix} = \begin{bmatrix} H_r \\ H_e \\ H_d \end{bmatrix} \quad (9)$$

The moment equation for a rotating frame is:

$$\bar{T} = \begin{bmatrix} \dot{H}_r + \omega_{Ae} H_d - \omega_{Ad} H_e \\ \dot{H}_e + \omega_{Ad} H_r - \omega_{Ar} H_d \\ \dot{H}_d + \omega_{Ar} H_e - \omega_{Ae} H_r \end{bmatrix} \quad (10)$$

The total torque applied about the gimbal  $e$ -axis is the  $e$ -component of matrix (10):

$$T_m = \dot{H}_e + \omega_{Ad} H_r - \omega_{Ar} H_d \quad (11)$$

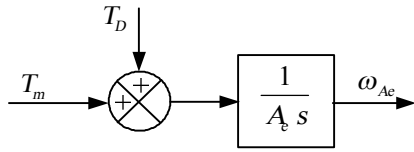


Figure 3. Gimbal motion equation

TABLE 1. Gyroscope characteristics

Characteristic	Value
Input rate	± 40 to ±1000 °/sec
output	AC or DC
Scale factor	Customer Specification
Natural frequency	20 to 140 Hz
Damping ratio	0.4 to 1.0

This equation can be obtained as a differential equation for the pitch angular velocity in the following form:

$$A_y \dot{\omega}_{Ae} = T_m + (A_d - A_y) \omega_{Ar} \omega_{Ad} + A_{yd} (\omega_{Ar}^2 - \omega_{Ad}^2) - A_{ye} (\dot{\omega}_{Ad} - \omega_{Ae} \omega_{Ar}) - A_{ye} (\dot{\omega}_{Ar} + \omega_{Ae} \omega_{Ad}) \tag{12}$$

$T_m$  represents the sum of the motor torque and external imperfection disturbance torques. Clearly then, from stabilization point of view, the "inertia terms" on the right represent unwanted disturbances. They will enter the control system in the same point as an external torque; consequently, they can be regarded as torque disturbance  $T_D$  (Figure 2):

$$T_D = (A_d - A_y) \omega_{Ar} \omega_{Ad} + A_{yd} (\omega_{Ar}^2 - \omega_{Ad}^2) - A_{ye} (\dot{\omega}_{Ad} - \omega_{Ae} \omega_{Ar}) - A_{ye} (\dot{\omega}_{Ar} + \omega_{Ae} \omega_{Ad}) \tag{13}$$

From the control point of view, it is suitable to let  $T_m$  represent only the motor torque. Therefore, Equation (12) can be represented by the block diagram in Figure 3. It is clear that the motor torque and the disturbance torques are inputs to an integrator which includes the moment of inertia  $A_y$ , and the output is the angular velocity  $\omega_{Ae}$ .

Equation (13) shows that the torque disturbance is caused by the base angular motion and the gimbal inertia parameters. Therefore, when the base is nonrotating ( $\omega_{pi} = \omega_{pj} = \omega_{pk} = 0$ ) the disturbance term is zero and just the motor torque  $T_m$  affects on the platform (stabilized object A). With regard to inertia parameters, it must be mentioned that the dynamic mass unbalance is the result of a non-symmetrical mass distribution called Product of Inertia (POI) [6]. The dynamic unbalance concept can be indicated by the inertia matrix. Therefore, if the considered gimbal has a symmetrical mass distribution with respect to its frame

axes, then the gimbal has no dynamic unbalance and its inertia matrix is diagonal. Also, if the gimbal has a non-symmetrical mass distribution with respect to its frame axes, then the gimbal has dynamic unbalance and its inertia matrix is not diagonal. Actually, in most papers, the model of gimbal system has been simplified using certain choices of inertia parameters to reduce the effects of dynamic mass unbalance which is considered an inevitable imperfection that can be encountered even in a well designed system. For example, in [4, 5], it has been assumed that the gimbal has no dynamic unbalance i.e.,  $A_{ye} = A_{yd} = A_{ye} = 0$ . When this assumption is applied on the gimbal model indicated in Equation (12), the equation of gimbal motion will be simplified to  $A_y \dot{\omega}_{Ae} = T_m + (A_d - A_y) \omega_{Ar} \omega_{Ad}$ . In this paper, it is assumed that the gimbal has dynamic mass unbalance, so the model indicated in Equation (12) will be interested.

#### 4. STABILIZATION LOOP CONSTRUCTION

It can be seen from Figure 2 that the stabilization loop is constituted of controller, DC motor, platform, and rate gyro. These components are identified as follows.

**4. 1. Rate Gyro** In this paper, the 475T rate gyroscope from the US Dynamics company is considered. The gyro has specifications shown in Table 1. The rate gyro can be modeled in the second order system typically as follows [12]:

$$G_{Gyro}(s) = \frac{\omega_n^2}{(s^2 + 2\zeta\omega_n s + \omega_n^2)} \tag{14}$$

Using the gyroscope dynamic specifications;  $\omega_n$  (Natural Frequency) = 50 Hz and  $\zeta$  (Damping Ratio) = 0.7, the transfer function is:

$$G_{Gyro}(s) = \frac{2500}{(s^2 + 70s + 2500)} \tag{15}$$

**4. 2. Platform** The platform represents the motor load which is attached to the shaft motor. The platform is modelled based on its moment of inertia  $J_L$  that depends on its dimensions and its position with respect to the axis of rotation. In this paper, a discussion is proposed to represent the platform, where its mass  $M=1kg$ , and radius  $r=14cm$ . Therefore, the moment of inertia is:

$$J_L = \frac{1}{2} Mr^2 = 9.8 \times 10^{-3} Kg.m^2 \tag{16}$$

**4. 3. Mathematical Model of DC Motor** The direct current (DC) motor is one of the simplest motor types. It

is widely preferred for high performance systems requiring minimum torque ripple, rapid dynamic torque, speed responses, high efficiency and good inertia [18]. These motors speedily respond to a command signal by means of a suitable controller [19]. In this kind of motors, the speed control is carried out by changing the supply voltage of the motor [20]. Development of a high performance controller to ensure reliable speed for systems is a topic of interest of many researchers [19]. Figure 4 shows the equivalent circuit of DC motor. DC motor can be described by a set of parameters and variables indicated in Table 2. The dynamic of the system can be represented by the following differential equations:

$$u_a(t) = R_a i_a(t) + L_a \frac{di_a}{dt} + e(t) \tag{17}$$

$$e(t) = K_e \omega_m(t) \tag{18}$$

$$T_m(t) = K_{TM} i_a(t) \tag{19}$$

$$T_m(t) = J_m^* \frac{d\omega_m}{dt} + a_m^* \omega_m(t) + T_D(t) \tag{20}$$

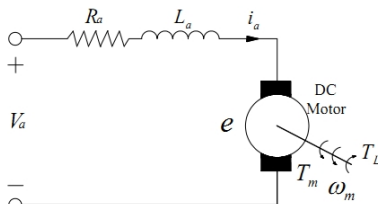


Figure 4. The equivalent circuit of DC motor [21]

TABLE 2. Parameters and variables of DC motor

Parameter	Value
$J_m$	Motor's moment of inertia
$a_m$	Motor's damping ratio
$R_a$	Resistance of the motor armature
$L_a$	Inductance of the motor armature
$J_L$	Platform's moment of inertia
$a_L$	Load's damping ratio
$K_e$	Motor electrical constant
$K_{TM}$	Motor mechanical constant
Variable	Value
$u_a$	Motor's armature voltage
$i_a$	DC motor armature current
$e$	Armature's inverse electromotive force
$\omega_m$	Motor's angular velocity
$T_m$	Torque generated by the motor
$T_L$	Torque applied at the platform
$T_D$	Torque disturbances

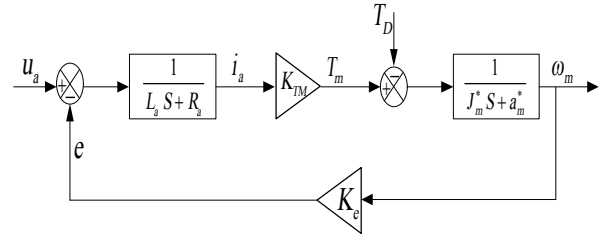


Figure 5. The block diagram of DC motor

In the last Equation (20),  $J_m^* = J_m + J_L$  represents the total moment of inertia seen from the motor side, whereas  $a_m^* = a_m + a_L$  is the total viscous friction constant seen from the motor side. By applying the Laplace transform to these equations when the initial conditions are taken as zero, the model of DC motor can be expressed as shown in Figure 5.

This system can be regarded as a MISO system with two inputs (voltage applied at the motor's armature and the external torque), and one output (platform's angular velocity), or it can be regarded as a SISO system neglecting  $T_D$  and the transfer function is:

$$G_m(s) = \frac{\omega_m(s)}{u_a(s)} = \frac{K_{TM}}{(L_a s + R_a) \cdot (J_m^* s + a_m^*) + K_e K_{TM}} \tag{21}$$

It is supposed that the platform must rotate at maximum angular velocity  $\omega = 2 \text{ rad/sec}$  in 35 m sec, so the motor must be able to accelerate it to  $\alpha = 56 \text{ rad/sec}^2$ . The torque required to produce this acceleration is:

$$T = J \cdot \alpha = 9.8 \times 10^{-3} \times 56 \approx 5.5 \text{ Nm} \tag{22}$$

The desired output power is:

$$P_{out} = T \cdot \omega = 5.5 \text{ Nm} \times 2 \text{ rad/sec} = 11 \text{ W} \tag{23}$$

For DC motor without gearbox (direct drive), we need a maximum torque to rotate the platform at  $\alpha = 56 \text{ rad/sec}^2$ . Therefore, DC motor from the NORTHROP GRUMMAN Company is proposed. The specifications of this DC motor are:

$$u_a = 27 \text{ V}, R_a = 4.5 \Omega, L_a = 0.003 \text{ H}$$

$$J_m = 0.0017 \text{ Kg m}^2, K_{TM} = 0.85 \text{ Nm/A}$$

$$K_e = 0.85 \text{ V/rad/sec}$$

Therefore, the transfer function of DC motor is:

$$G_m(s) = \frac{24637.68}{s^2 + 1500s + 20942}; a_m^* = 0 \tag{24}$$

The DC motor time response is shown in Figure 6.

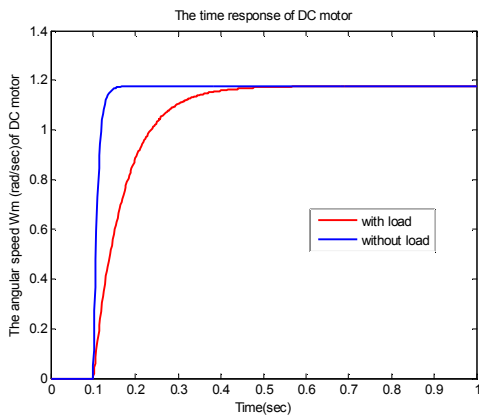


Figure 6. DC motor time response

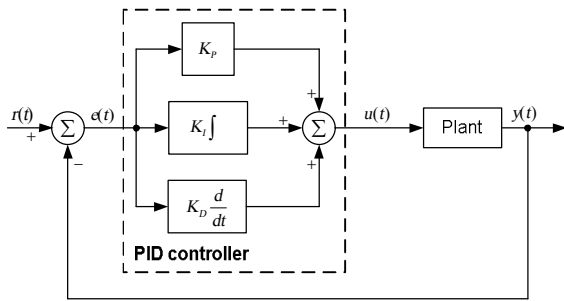


Figure 7. PID control system

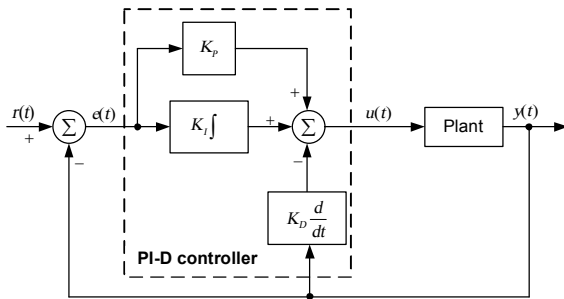


Figure 8. PI-D control system

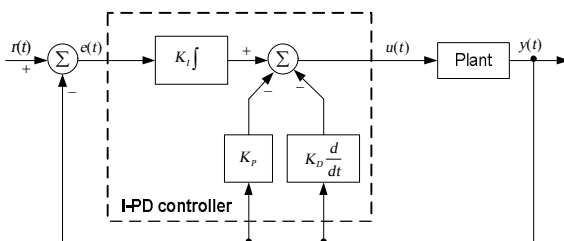


Figure 9. I-PD control system

**4. 4. Controller Design** If gimbal design is not proper, the control algorithms may become complex and it may not be possible to meet the performance criteria [22]. While the well-designed gimbal assembly reduces

the jitter of sensor's line of sight and hence needs a simpler control system [22, 23] which simplifies the implementation of control laws in real time. Due to the simplicity of PID controller, it has been selected in addition to three of its structures to be investigated in this paper. PID controller algorithm is given by:

$$u(t) = K_p e(t) + K_i \int e(\tau) d\tau + K_D \frac{de(t)}{dt}$$

$$u(t) = K_p \left[ e(t) + \frac{1}{T_i} \int e(\tau) d\tau + T_D \frac{de(t)}{dt} \right] \tag{25}$$

Control signal  $u(t)$  is a linear combination of error  $e(t)$ , its integral and derivative, where  $K_p$  is proportional gain,  $K_i$  is integral gain,  $K_D$  is derivative gain,  $T_i$  is integral time, and  $T_D$  is derivative time.

Figure 7 shows the schematic model of a control system with a PID controller. The classical structure of PID controller can be converted into many different forms utilizing the cascade control approach so that these forms are able to be applied in some applications. Because of possible discontinuity (step change) in reference signal that are transferred into error signal and result in impulse travelling through derivative channel and thus cause large control signals  $u(t)$ , it is more suitable in practical implementation to use "derivative of output controller form" (PI-D) shown in Figure 8.

It is even more suitable controller structure if there exist sensors that give that information, such as tachometers in electromechanical servo systems or rate gyro in mobile objects control. If PI-D structure (Figure. 8) is used, discontinuity in  $r(t)$  will be still transferred through proportional into control signal  $u(t)$ , but it will not have so strong effect as if it was amplified by derivative element. PI-D controller algorithm is given by:

$$u(t) = K_p e(t) + K_i \int e(\tau) d\tau - K_D \frac{dy(t)}{dt} \tag{26}$$

The set-point-on-I-only controller (I-PD form) shown in Figure 9 is not so often as PI-D structure, but it has certain advantages. I-PD controller algorithm is given by:

$$u(t) = K_p y(t) + K_i \int e(\tau) d\tau - K_D \frac{dy(t)}{dt} \tag{27}$$

With this structure transfer of reference value discontinuities to control signal is completely avoided. Control signal has less sharp changes than other structures. Serial (interactive) structure (PD\*PI form) is very often in process industry. I channel uses both the error signal  $e(t)$  and derivative of the error signal  $de(t)/dt$ . PD\*PI controller block diagram is shown in Figure 10. It is realized as serial connection of PD and PI controller. PD\*PI control algorithm is:

$$u(t) = K_p^s e_1(t) + K_I^s \int e_1(\tau) d\tau ; e_1(t) = e(t) + T_D^s \frac{de(t)}{dt} \quad (28)$$

**5. SIMULATION AND RESULTS**

Before beginning of simulation, there are some ideas and concepts which must be confirmed, clarified and specified.

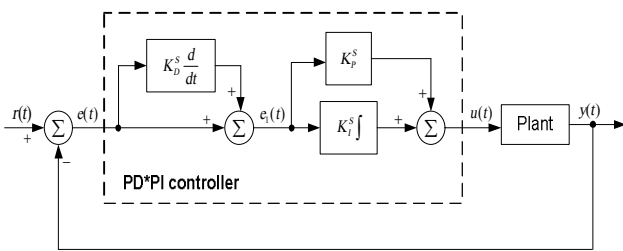


**Figure 10. PD\*PI control system**

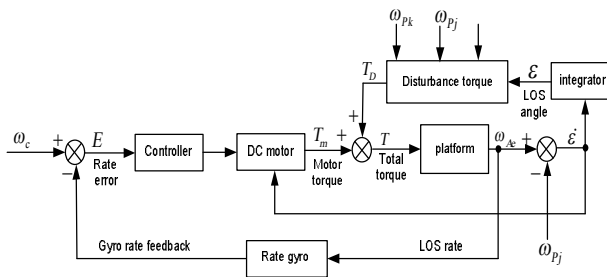


**Figure 11. Simulink model of servo control system**

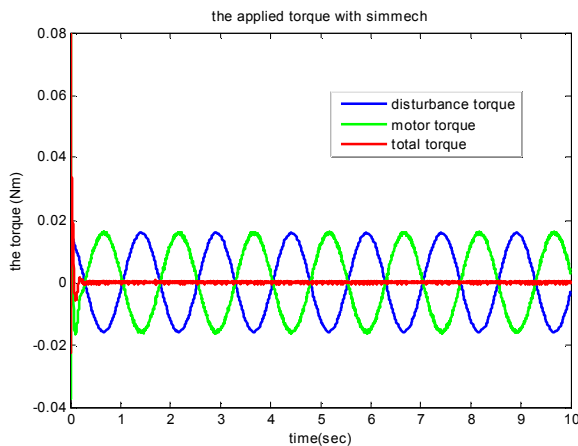


**Figure 12. The total applied torque**

- ❖ It was mentioned in Equation (13) that the torque disturbance is zero when the base is nonrotating ( $\omega_{p_i} = \omega_{p_j} = \omega_{p_k} = 0$ ).
- ❖ The geometric properties of the gimbal mechanism (Figure 1) indicates that the rate  $\omega_{p_j}$  is the most dominant parameter in the torque disturbance term  $T_D$ . Therefore, this parameter will be interested and taken into account as a variable value.
- ❖ The total moment of inertia seen from the motor side is  $J_m + J_L = 11.5 \times 10^{-3} \text{ kg.m}^2$ .
- ❖ In order to take into account the effect of base angular motion, the rate  $\dot{\epsilon}$  (Equation 6-b) must be fed back to the DC motor through the motor electrical constant (back emf constant).
- ❖ In the simulation tests, the following values are considered; the input rate is  $\omega_c = 20 \text{ deg/sec}$  while ( $\omega_{p_k} = 10, \omega_{p_i} = 5$ ) deg/sec and  $\omega_{p_j}$  changes from zero to 35 deg/sec.

Based on what has carried out above, the complete simulink model of servo control system introduced can be constructed using MATLAB as shown in Figure 11. The model shown in Figure 11 is built using MATLAB/Simulink utilizing the four controllers discussed above; conventional PID, PI-D controller, I-PD controller, and PD\*PI controller with ( $K_p = 0.96, K_I = 10.7, K_D = 0.0001$ ) which were adjusted using Ziegler-Nichols method. At first, using PID controller, it is useful to graphically illustrate the principle of gimbal system work which depends on Newton's second law (Equation 1), then to ensure that the control system, which has been built utilizing the gimbal model obtained in Equation (12), can accurately provide stability to the object A. The diagrams indicated in Figure 12 show how the closed-loop control system generates a control torque at the motor that is equal and opposite to the net disturbance torque. Therefore, the object is prevented from rotating with respect to the inertial space. Afterwards, the time step response of the servo control system for these four controllers are obtained and drawn on one plane. The numerical simulations are performed in order to investigate the performance of the proposed cascade controllers in terms of the performance criteria. The desired performance requirements of the servo system proposed are:

- ❖ Rise time  $t_r \leq 0.2 \text{ sec}$ .
- ❖ Settling time  $t_s \leq 0.35 \text{ sec}$ .
- ❖ Maximum overshoot  $M_p \leq 20\%$ .
- ❖ Steady state error  $e_{ss} = 0$ .

These criteria must generally be satisfied in any control system.

Table 3 shows the values of the performance criteria obtained with the adjusted controller parameters. It is

noted that all controllers proposed realize a zero steady state error and all the controllers PID, PI-D, PD\*PI have the same performance as shown in Figures (13-20).

Table 3 displays that the I-PD controller realizes a better performance compared with the other controllers. It is clear that the I-PD controller maintain an acceptable overshoot despite of  $\omega_{pj}$  magnitude increasing. In contrast, for the other controllers, the overshoot appears when  $\omega_{pj} = 5$  deg/sec and increases as  $\omega_{pj}$  magnitude increases. It exceeds the desired overshoot limit when  $\omega_{pj} = 15$  deg/sec .

The drawback of the I-PD controller is just when  $\omega_{pj}$  is little ( $\omega_{pj} = 0-15$  deg/sec) the system response is slightly slow and the settling time is somewhat more than the desired value ( $t_s = 0.35$  sec) .

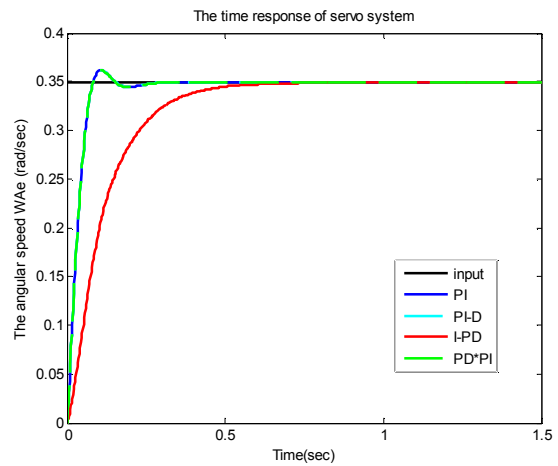


Figure 14. Servo system response for  $\omega_{pj} = 5$  deg/sec

TABLE 3. Simulation results for ( $K_p = 0.96, K_i = 10.7, K_d = 0.0001$ )

$\omega_{pj}$ deg/s	PID , PI-D , PD*PI			I-PD		
	$t_s$ sec	$t_r$ sec	$M_p$ %	$t_s$ sec	$t_r$ sec	$M_p$ %
0	0.29	0.08	0	0.46	0.25	0
5	0.14	0.06	3.4	0.43	0.24	0
10	0.21	0.05	14.3	0.41	0.23	0
15	0.42	0.05	24.3	0.37	0.19	0
20	0.45	0.04	35	0.31	0.11	0
25	0.51	0.03	46.7	0.24	0.08	0
30	0.56	0.03	58.1	0.18	0.06	7.7
35	0.62	0.03	69.4	0.35	0.05	18.1

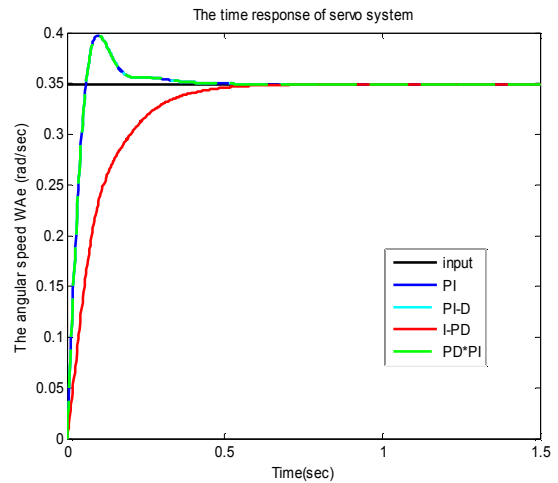


Figure 15. Servo system response for  $\omega_{pj} = 10$  deg/sec

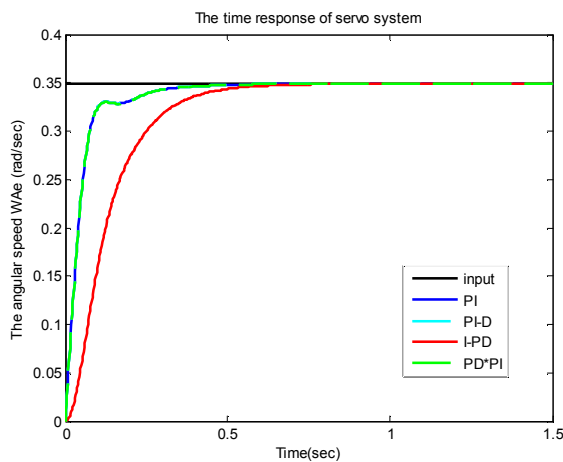


Figure 13. Servo system response for  $\omega_{pj} = 0$  deg/sec

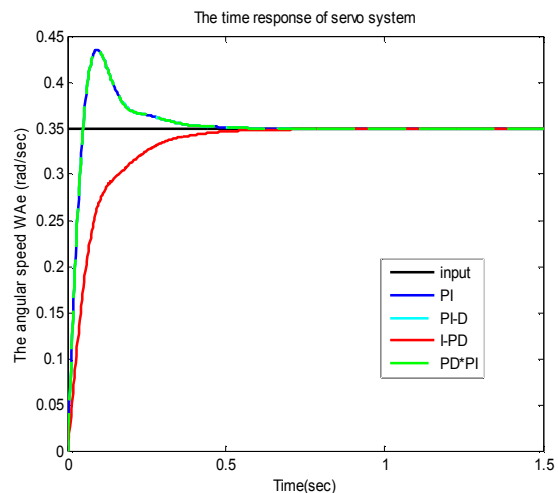


Figure 16. Servo system response for  $\omega_{pj} = 15$  deg/sec

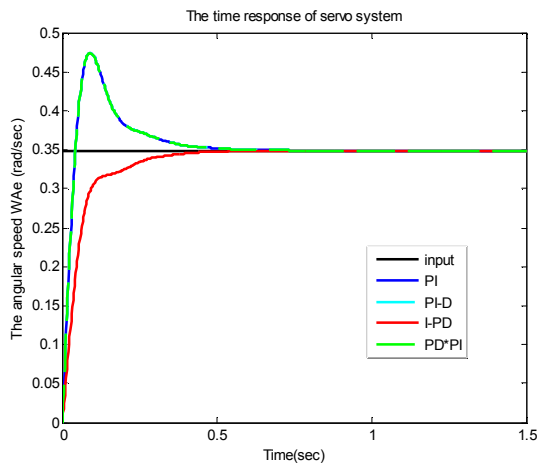


Figure 17. Servo system response for  $\omega_{pj} = 20 \text{ deg/sec}$

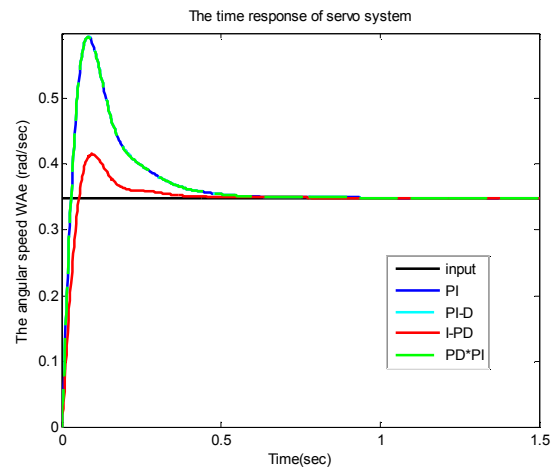


Figure 20. Servo system response for  $\omega_{pj} = 35 \text{ deg/sec}$

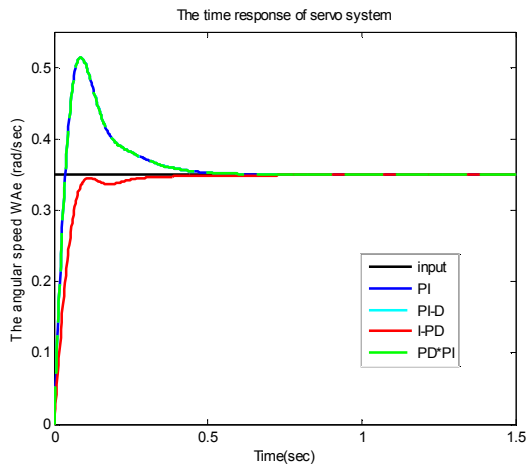


Figure 18. Servo system response for  $\omega_{pj} = 25 \text{ deg/sec}$

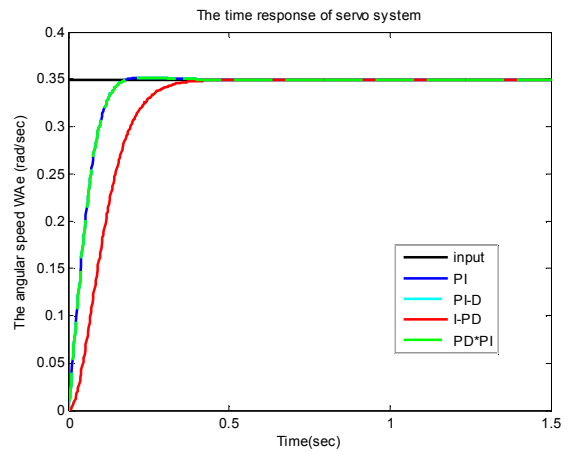


Figure 21. Servo system response for  $\omega_{pj} = 0 \text{ deg/sec}$

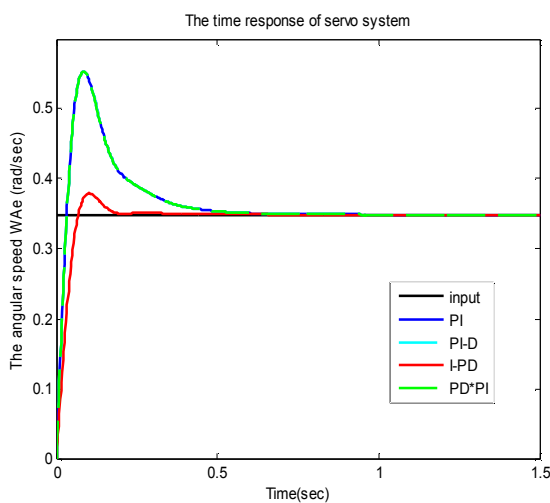


Figure 19. Servo system response for  $\omega_{pj} = 30 \text{ deg/sec}$

TABLE 4. Simulation results for ( $K_p=0.7, K_i=10.7, K_d=0.0001$ )

$\omega_{pj}$ deg/s	PID , PI-D , PD*PI			I-PD		
	$t_s$ sec	$t_r$ sec	$M_p$ %	$t_s$ sec	$t_r$ sec	$M_p$ %
0	0.15	0.1	1.7	0.3	0.18	0
5	0.1	0.07	5.63	0.28	0.17	0
10	0.35	0.06	14.29	0.24	0.15	0
15	0.33	0.05	24.49	0.17	0.13	0
20	0.37	0.04	35.5	0.27	0.08	3.69
25	0.45	0.04	47	0.36	0.06	11.63
30	0.46	0.03	58.83	0.42	0.05	21.4
35	0.47	0.03	70.86	0.45	0.04	32.29

This drawback of the I-PD controller can be solved if the coefficient  $K_p$  is readjusted. Therefore, the same

simulation tests have been repeated utilizing another value for the proportional gain ( $K_p = 0.7$ ) and the results are indicated in Table 4 and Figures (21-28).

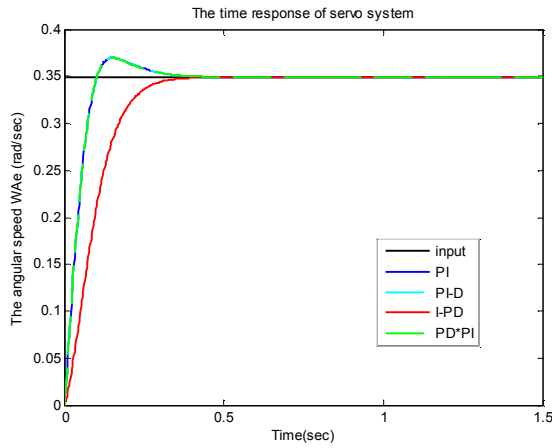


Figure 22. Servo system response for  $\omega_{pj} = 5$  deg/sec

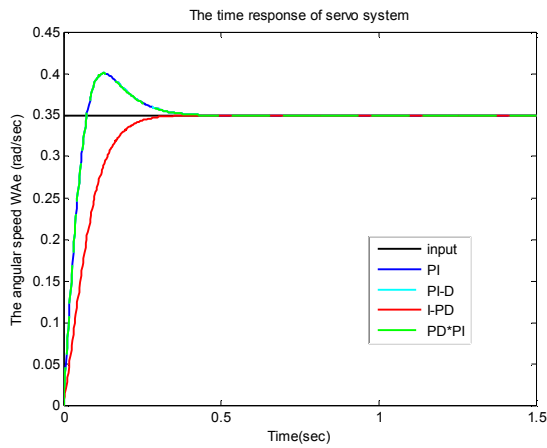


Figure 23. Servo system response for  $\omega_{pj} = 10$  deg/sec

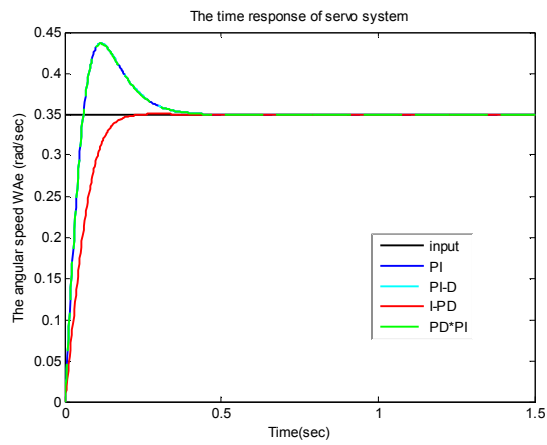


Figure 24. Servo system response for  $\omega_{pj} = 15$  deg/sec

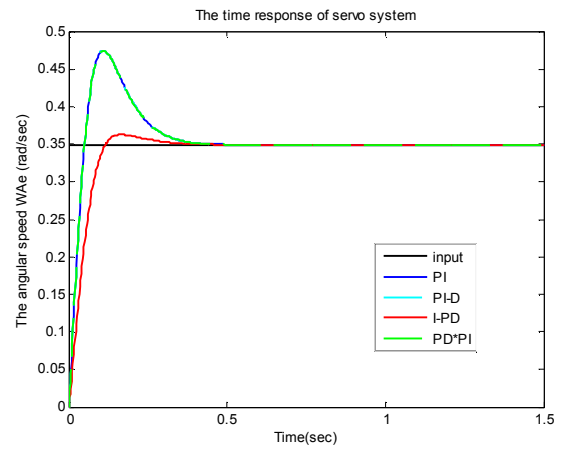


Figure 25. Servo system response for  $\omega_{pj} = 20$  deg/sec

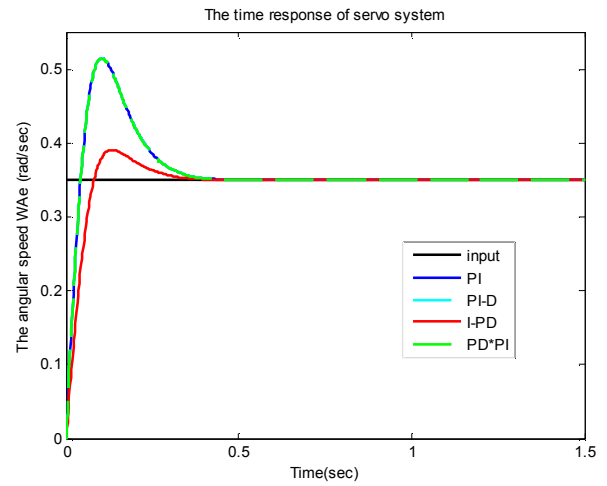


Figure 26. Servo system response for  $\omega_{pj} = 25$  deg/sec

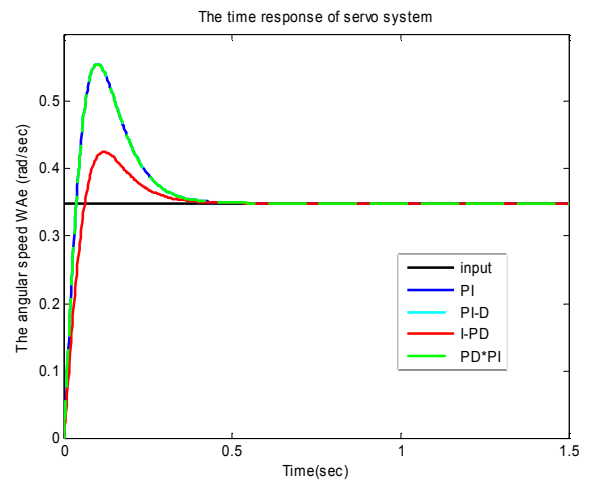


Figure 27. Servo system response for  $\omega_{pj} = 30$  deg/sec

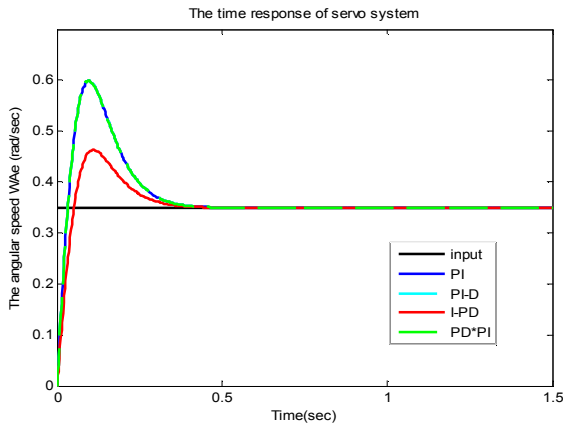


Figure 28. Servo system response for  $\omega_{pj} = 35 \text{ deg/sec}$

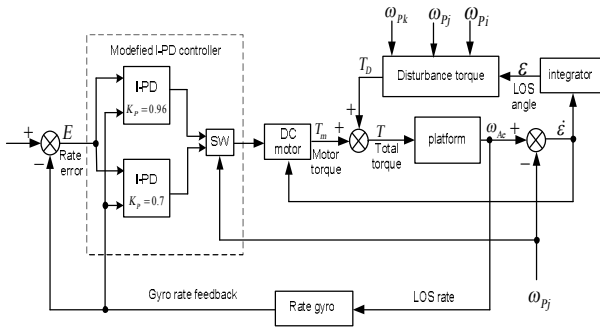


Figure 29. Servo system with modified I-PD controller

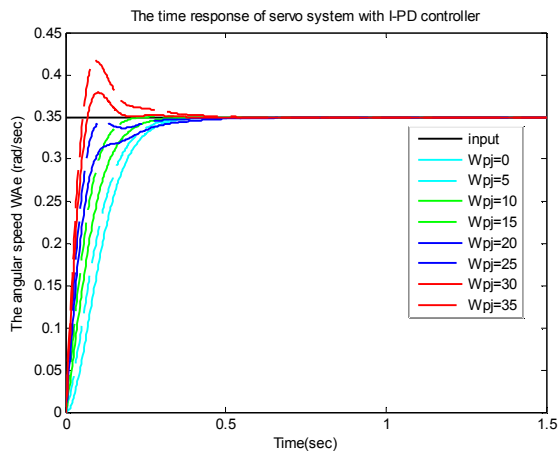


Figure 30. Servo system response using modified I-PD

Even after readjusting operation, the PID, PI-D, and PD\*PI controllers are still disable to give the desired response. While the readjusted I-PD controller improves the system performance especially decreasing the settling time when  $\omega_{pj} = 0 - 15 \text{ deg/sec}$ .

The performance criteria indicated in the bordered quarters of Tables 3 and 4 confirm that the better controller is the I-PD controller which shortens the step response settling time often without overshoot which is considered unwanted in such a servo control systems. Furthermore, I-PD controller does not require advanced mathematics to design and can be easily adjusted (or "tuned") to the desired application, unlike more complicated control algorithms based on optimal control theory. Based on what has been carried out above, two observations can be highlighted:

- ❖ Simulation results indicated in Tables 3 and 4 indicate that the coefficient  $K_p$  of the I-PD controller is the key parameter that guarantees an acceptable performance when it is correctly readjusted.
- ❖ Figure 1 shows that the gimbal can be rotated about the gimbal  $e$ -axis which is identical with the base  $j$ -axis. Thus, it can be concluded that the rate  $\omega_{pj}$  is the most dominant variable which directly affects the gimbal system performance.

Therefore, based on these observations, the servo control system introduced in Figure 11 is modified so that the controller is reconstructed utilizing two parallel I-PD controllers, one with  $K_p = 0.7$  for the range  $\omega_{pj} = [0 - 15] \text{ deg/sec}$  and the other with  $K_p = 0.96$  for the range  $\omega_{pj} = [16 - 35] \text{ deg/sec}$ . In the modified controller, the value  $\omega_{pj} = 15 \text{ deg/sec}$  is regarded as a threshold value which is used to change the utilized controller according to the value of  $\omega_{pj}$ . This modification improves the control system performance and provides good adaptability for the gimbal system against changes of the base angular rates which are considered important operational conditions that form a significant source of torque disturbances. The modified servo control system and its step time response are shown in Figures 29 and 30, respectively. It is clear that the modified I-PD controller gives the best performance compared with the other controllers along the whole range of the base angular rate  $\omega_{pj} = [0 - 35] \text{ deg/sec}$ .

### 6. CONCLUSION

In this paper, a servo control system for one axis gimbal mechanism is introduced. The gimbal motion equation is derived by taking into account the torque disturbance results from the base angular motion. Then, the stabilization loop is constructed. The conventional PID controller, P-ID controller, PD\*PI controller, and I-PD controller are investigated and utilized in the stabilization loop structure. The servo control system obtained is simulated using MATLAB/Simulink tool and many simulation tests are carried out. The results of

each controller are discussed and analyzed in terms of performance criteria. It can be seen that PID, P-ID, and PD\*PI controllers have the same performance where all of them create an increased overshoot whenever the angular rate  $\omega_{p_j}$  increases. On the other hand, the I-PD structure absolutely prevents the transfer of reference value discontinuities to control signal and the control signal has less sharp changes than other structures. Therefore, this controller realizes acceptable performance with less overshoot and suitable settling time. Thus, the servo control system is reconstructed utilizing the modified I-PD controller.

## 7. REFERENCES

- Masten, M. K., "Inertially stabilized platforms for optical imaging systems", *Control Systems, IEEE*, Vol. 28, No. 1, (2008), 47-64.
- Hilkert, J., "Inertially stabilized platform technology concepts and principles", *Control Systems, IEEE*, Vol. 28, No. 1, (2008), 26-46.
- Singh, R., Hanmandlu, M., Khatoon, S. and Madsu, V. K., "Modeling and simulation of the dynamics of a large size stabilized gimbal platform assembly", Vol. 1, (2008), 111-119.
- Rue, A., "Precision stabilization systems", *Aerospace and Electronic Systems, IEEE Transactions on*, No. 1, (1974), 34-42.
- Ekstrand, B., "Equations of motion for a two-axes gimbal system", *Aerospace and Electronic Systems, IEEE Transactions on*, Vol. 37, No. 3, (2001), 1083-1091.
- Otowski, D. R., Wiener, K. and Rathbun, B. A., "Mass properties factors in achieving stable imagery from a gimbal mounted camera", in SPIE Defense and Security Symposium, International Society for Optics and Photonics. (2008), 69460B-69460B-13.
- Makableh, Y., "Efficient control of dc servomotor systems using backpropagation neural networks", (2011).
- Korayem, M. H., Ahmadi, R., Jaafari, N., Jamali, Y. and Kiomarsi, M., "Design, modeling, implementation and experimental analysis of 6r robot", *International Journal of Engineering*, Vol. 21, (2008), 71-78.
- Akar, M. and Temiz, I., "Motion controller design for the speed control of dc servo motor", *International Journal of Applied Mathematics and Informatics*, Vol. 4, No. 1, (2007), 131-137.
- Rigatos, G. G., "Adaptive fuzzy control of dc motors using state and output feedback", *Electric Power Systems Research*, Vol. 79, No. 11, (2009), 1579-1592.
- Rigatos, G. G., "Particle and kalman filtering for state estimation and control of dc motors", *ISA Transactions*, Vol. 48, No. 1, (2009), 62-72.
- Lee, H.-P. and Yoo, I.-E., "Robust control design for a two-axis gimbale stabilization system", in Aerospace Conference, IEEE., (2008), 1-7.
- Shuang, Y. and Yanzheng, Z., "A new measurement method for unbalanced moments in a two-axis gimbale seeker", *Chinese Journal of Aeronautics*, Vol. 23, No. 1, (2010), 117-122.
- Hasturk, O., Erkmen, A. M. and Erkmen, İ., "Proxy-based sliding mode stabilization of a two-axis gimbale platform", *Target*, Vol. 3, No. 4. (2011)
- Khodadadi, H., Motlagh, M. R. J. and Gorji, M., "Robust control and modeling a 2-dof inertial stabilized platform", in Electrical, Control and Computer Engineering (INECCE), International Conference on, IEEE. (2011), 223-228.
- Tang, K., Huang, S., Tan, K. and Lee, T., "Combined pid and adaptive nonlinear control for servo mechanical systems", *Mechatronics*, Vol. 14, No. 6, (2004), 701-714.
- Malaysia, M., "Non-linear modeling and cascade control of an industrial pneumatic actuator system", *Australian Journal of Basic and Applied Sciences*, Vol. 5, No. 8, (2011), 465-477.
- Malhotra, R., Singh, N. and Singh, Y., "Design of embedded hybrid fuzzy-ga control strategy for speed control of dc motor: A servo control case study", *International Journal of Computer Applications*, Vol. 6, No. 5, (2010), 37-46.
- Abjadi, N., Soltani, J., Pahlavaninizhad, M. and Askari, J., "A nonlinear adaptive controller for speed sensorless pmsm taking the iron loss resistance into account", in Electrical Machines and Systems, ICEMS Proceedings of the Eighth International Conference on, IEEE. Vol. 1, (2005), 188-193.
- Khajorntraidet, C. and Srisertpol, J., "Torque control for dc servo motor using adaptive load torque compensation", in Proceedings of the 9th WSEAS international conference on System science and simulation in engineering, World Scientific and Engineering Academy and Society (WSEAS). (2010), 454-458.
- Akar, M., Hekim, M., Temiz, I. and Dogan, Z., "The speed and torque control of direct current servo motors by using cascade fuzzy pi controller", *Przegląd Elektrotechniczny Selected full Texts*, Vol. 88, No. 5b, (2012), 123-127.
- Masten, M. K. and Hilkert, J., "Electromechanical system configurations for pointing, tracking, and stabilization applications", in Technical Symposium Southeast, International Society for Optics and Photonics. (1987), 75-87.
- Stokum, L. A. and Carroll, G. R., "Precision stabilized platform for shipborne electro-optical systems", *SPIE*, Vol. 493, (1984), 414-425.

## Modeling, Control and Simulation of Cascade Control Servo System for One Axis Gimbal Mechanism

M. Abdo<sup>a</sup>, A. R. Toloei<sup>b</sup>, A. R. Vali<sup>b</sup>, M. R. Arvan<sup>b</sup>

<sup>a</sup> Department of Electrical Engineering, Malek-Ashtar University of Technology, Tehran, Iran

<sup>b</sup> Department of Aerospace, Shahid Beheshti University, Tehran, Iran

### PAPER INFO

### چکیده

#### Paper history:

Received 27 March 2013

Received in revised form 27 April 2013

Accepted 20 June 2013

#### Keywords:

Gimbal System  
Rtae Gyro  
Line of Sight  
Stabilization Loop  
Servo System  
DC Motor

به منظور تامین پایداری یک جسم قرار داده شده بر روی طوقه، از سیستم مکانیزم پایدارسازی طوقه استفاده می‌شود. این مکانیزم بر مبنای ایزوله کردن جسم از حرکت زاویه‌ای و لرزش مبنا عمل می‌نماید. در این مقاله، یک مدل کنترل سیستم سروو برای مکانیزم طوقه یک درجه آزادی با استفاده از کنترل‌کننده‌های تناسبی-مشتقی-انتگرالی آبشاری (Cascade PID) ارائه شده است. روابط گشتاور طوقه‌ها در نظر گرفتن حرکت زاویه‌ای مبنا استخراج شده و ساختار کنترل‌کننده PID معمول و سه ساختار متفاوت کنترل‌کننده PID آبشاری مورد بررسی قرار گرفته است. حلقه کنترلی سروو با استفاده از کنترل‌کننده‌های فوق در محیط نرم‌افزار MATLAB/Simulink مدلسازی شده است. نتایج حاصل از شبیه‌سازی مقایسه و کارایی سیستم سروو با اندازه‌گیری معیارهای عملکرد سیستم در هر یک از این حالات مورد بررسی قرار گرفته است. مقایسه این نتایج نشان می‌دهد که بیشترین کارایی بهبود داده شده با استفاده از کنترل‌کننده I-PD حاصل شده است. نوآوری این مقاله در طراحی یک سیستم کنترل سروو با استفاده از کنترل‌کننده اصلاح شده می‌باشد که شامل دو کنترل‌کننده I-PD موازی است. این کنترل‌کننده‌ها با استفاده از یک سوئیچ دارای مقدار آستانه فرمان می‌گیرند. نتایج حاصل از شبیه‌سازی این ساختار، نشان می‌دهد که کنترل‌کننده پیشنهادی الزامات یک سیستم سروو مطابقت را برآورده کرده است.

doi: 10.5829/idosi.ije.2014.27.01a.18

